Master's Thesis

Synthesis and Characterization of a Biologically Active Self-Assembling Block Copolymer

Thesis for Obtaining the Degree
Master of Science
Major in Nanoscience

Kasper Renggli

supervised by Dr. C. Vebert and Prof. Dr. W. Meier
Department of Chemistry
University of Basel

July 20, 2009

Abstract

In this master's thesis an amphiphilic nucleotide-based block copolymer was synthesized using solid phase synthesis. We used a biologically active DNA sequence which is involved in infection by the vesicular stomatitis virus. As the hydrophobic, non-polar segment, *poly*(butadiene) was selected because of its low polydispersity and terminal modification. The copolymer and its self-assembly in dilute aqueous solution was studied by FTIR, CD spectroscopy, UV/Vis spectroscopy, DLS, SEM and AFM. Furthermore, we performed preliminary biological assays in order to test the bio-compatibility and the cellular uptake of the nucleotide-based synthesized copolymer, using THP-1 human acute monocytic leukemia cells. These cell experiments were executed in comparison to the biologically inert PB-PEG which was characterized by GPC, DLS/SLS and TEM. Incubation of THP-1 cancer cells with biologically active self-assembling copolymers shows that the growth of THP-1 cells is reduced without a toxic effect.

Contents

CHAPTER 1

Introduction

In the last years the preparation of self-assembled structures in the nanometer scale has aroused the interest of the scientific world. Molecular self-assembly is the spontaneous association of molecules under equilibrium conditions into stable, structurally well-defined aggregates hold by non-covalent interactions. Well known for several years are lipid molecules and there ability to form liposomes or vesicles through self-assembly in aqueous solution [28]. These structures have found there way into many scientific and applied fields [15, 32]. A problem of these self-assembled structures is that they are very instable and biologically inert [2]. The instability as well as the biological function can be enhanced by using different approaches.

One method to form nanometer scale structures is to use amphiphilic block copolymers. Our group developed a new approach, using a nucleotide sequence as the water-soluble polymer segment to build a biologically active amphiphilic block copolymer [13]. Driven by the chemical incompatibility between the two covalently linked hydrophobic and hydrophilic segments, block copolymers undergo self-assembly in aqueous solution. This process is currently the most versatile approach to control and drive the organization of polymers at the nanometer length scale [8]. They form structures such as bilayers, micelles and vesicles also called polymersomes depending on the composition of the molecules [7]. The presence of the DNA[1] sequence in these molecules is expected to yield functional biologically active self-assemblies. When composing the outer shell of a vesicle it is possible to hybridize the single stranded DNA with its complementary sequence. The approach using vesicles is driven by the foreseen possibility of encapsulation and the delivery of drugs by functionalized vesicles [22]. Thus, they act as bio-reactors and the chance of vesicle fusion could be interesting for cell studies in order to deliver a drug via specific receptors on cell membranes [11, 29].

During this master's project an amphiphilic nucleotide-based block copolymers was synthesized using solid phase synthesis [13]. In contrast to Teixeira et al. we used a biologically active DNA sequence (*3'*-AACTGAGATGGCGGATGAAGG-*5'*) reported by Luyet et al. [19]. This DNA segment which mediates receptor sorting into multivesicular endosomes is necessary for infection by the vesicular stomatitis virus which infects cells through the endosome.

1 Desoxyribonucleic Acid

Poly(butadiene) was selected as the hydrophobic, non-polar segment because of its low polydispersity and terminal modification, which is an essential prerequisite to link the hydrophilic and the hydrophobic parts.
The copolymer was characterized by fourier transform infrared spectroscopy, circular dichroism, UV/Vis spectroscopy, dynamic light scattering, scanning electron microscopy and atomic force microscopy. Additionally *poly*(butadiene)-b-*poly*(ethylene-glycol) an amphiphilic biologically inert block copolymer provided by the group of Axel Müller in Bayreuth was characterized by gel permeation chromatography, dynamic- and static light scattering as well as transmission electron microscopy in order to use it as a control for cell experiments.
Furthermore, we performed preliminary biological assays to test the bio-compatibility and the cellular uptake of the nucleotide-based synthesized copolymer in comparison to PB[1]-PEG[2], using THP-1 human acute monocytic leukemia cells. These well studied cancer cells with distinct monocytic markers can be differentiated into macrophage-like cells and are very suitable for complete cell studies [31].

1 *Poly*(Butadiene)
2 *Poly*(Ethylene-Glycol)

CHAPTER 2

Materials and Methods

2.1 Solid Phase Synthesis of PB_{2000}-siDNA

We performed a solid phase synthesis within a reaction reactor with a volume of approximately 2 $m\ell$ as reported earlier by Teixeira et al. [13]. A hydrophilic 21-meric single-stranded DNA oligonucleotide sequence purchased from Microsynth AG, Switzerland was used. It is attached via a C_{10}-linker to a carboxylic acid: *3'*-AACTGAGATGGCGGATGAAGG-*5'*-C_{10}-COOH (we will refer to the 21-meric DNA as siDNA[1]). As a hydrophobic part we used *poly*(butadiene) produced by the group of Axel Müller in Bayreuth. This copolymer is functionalized with an amino group: PB_{2000}-NH_2. DIC[2] was used as initiator and DCM[3] as solvent.
According to the mechanism shown in figure 2.1, the coupling reagent DIC is used to activate the carboxylic acid. The resulting ester is now activated for a nucleophilic attack due to the fact that substitution with the nucleophile, in our case PB_{2000}-NH_2, leads to a stable urea as a leaving group.

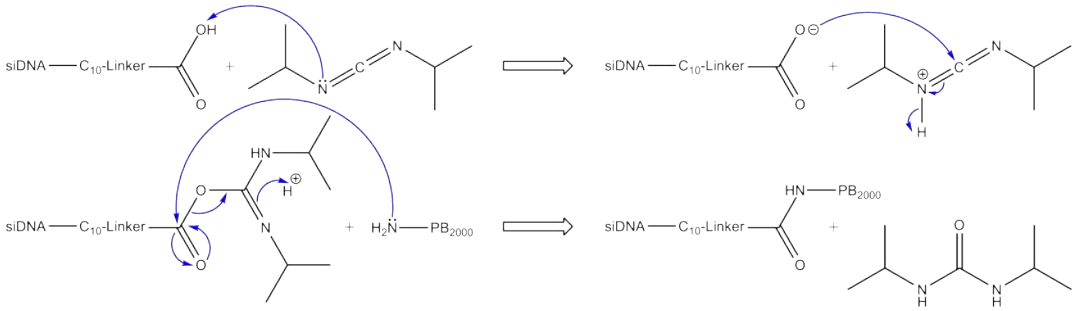

Figure 2.1: Mechanism of the solid phase synthesis. DIC activates the carboxylic acid and the resulting ester is submitted to a nucleophilic attack by the amino group of the *poly*(butadiene).

1 Small Interfering DNA
2 Diisopropylcarbodiimide
3 Dichloromethane

As mentioned above, the nucleotide-based block copolymer was synthesized at room temperature inside a 2 $m\ell$ reaction reactor. siDNA-C_{10}-COOH ($M_w = 6900\ g \cdot mol^{-1}$, 20.7 mg, 3 μmol, 1 eq) was added together with DIC ($M_w = 126.2\ g \cdot mol^{-1}$, 454.5 μg, 0.6 $\mu\ell$, 1.2 eq) to a solution of PB_{2000}-NH_2 ($M_w = 3500\ g \cdot mol^{-1}$, 52.5 mg, 5 eq) in 1.5 $m\ell$ DCM.
The solution was shaken overnight and afterwards washed several times with DCM to get rid of the initiator (DIC) and the non-reacted material. As a cleavage step 1.5 $m\ell$ of a 33% NH_4OH was added and transferred to an eppendorf tube where it was shaken overnight at a temperature of 40 $°C$. The ammonium hydroxide cleaves the oligonucleotides from the solid support and the content is then filtered away. To separate the PB_{2000}-siDNA from the free unreacted oligonucleotides a SEC[1] was carried out using Sephadex©G-50 and buffer (150 mM NaCl and 0.01% Azide). The SEC detects the presence of DNA at an UV[2] absorbtion wavelength of 280 nm. This UV sensitivity of the copolymer further leads to accurate concentration determination (see section 2.3 and 2.5).
The different fractions collected from SEC were then lyophilized overnight in order to remove the remaining buffer (procedure is explained in section 2.2). As a last step we dialyzed the product within dialysis cassettes with a MWCO[3] of 3500 Da to filter out the salt of the buffer as well as the remaining ammonium hydroxide from the cleavage step (concept shown in section 2.4).
The synthesis resulted in 10 mg copolymer. This corresponds to 1 μmol of PB-siDNA ($M_w = 10400\ g \cdot mol$) and to a yield of 32%. Note that the actual yield should be higher due to the fact that we lost some material in the lyophilization process.

2.2 Lyophilization

The basic principle behind lyophilization is to remove the water without loosing the material. For that purpose we use the fact that the liquid phase of water can be eliminated upon sublimation from solid to gas phase. First the sample is shock frozen in liquid nitrogen (77.35 K) and put into a low-pressure chamber at 5 $mbar$. This can be done either in a flask or in an eppendorf tube which is centrifuged to support the process.

2.3 Size Exclusion Chromatography

SEC is a liquid chromatography technique which separates solutes from each other depending on their hydrodynamic volume, this does not involve physical or chemical interactions. The stationary phase consists of Sephadex©G-50 beads (GE Healthcare, UK) with pore sizes between 50 μm and 150 μm. The pores in these beads are trapping molecules with molecular weights between 1500 $g \cdot mol^{-1}$ and 30000 $g \cdot mol^{-1}$. Larger molecules can not access some of the pores and exit the column more rapidly. Smaller molecules penetrate into more of the porous structure and elute at longer retention times. It is this filtration effect which causes separation by size.

1 Size Exclusion Chromatography
2 Ultraviolet
3 Molecular Weight Cut-Off

2.3.1 Gel Permeation Chromatography

GPC[1] is a separation technique to determine the molecular weight and the PDI[2] of polymers [33]. To determine the molecular weight, a series of standards of known molecular weight is analyzed. The retention time for these standards is used to create a calibration curve. With its help, the retention time for an unknown material can then be determined based on the retention volume at which it elutes. The results of this analysis are typically displayed as the molecular weight distribution and due to that we can estimate the PDI.
We used GPC to determine the molecular weight and the PDI of the PB-PEG block copolymer. As a standard we used *poly*(butadiene) in chloroform to create the calibration curve (see appendix A). The setup is using a refractive index detector and according to that the resulting data is given as intensity versus volume.

2.3.1.1 Sample Preparation

Since the column is chloroform driven, the polymer has to be dissolved in the same solvent. We work with a concentration of 4 $mg \cdot m\ell^{-1}$ and prepare usually about 2 $m\ell$. This solution is shaken overnight to ensure that all the material is dissolved properly. The content is then transferred into a syringe and filtered. The first about 0.5 $m\ell$ are trashed to get rid of dust particles or impurities which are coming from the filter and/or the syringe. The remaining solution of $\sim$ 1.5 $m\ell$ is then filtered into a GPC vial and is ready to be measured.

2.4 Dialysis

Dialysis is an easy and straight forward way to purify copolymers with a sample recovery of more than 95% [20]. The dissolved material is added to dialysis cassettes purchased from Slide-A-Lyzer Dialysis Products, Thermo Fisher Scientific, USA.
By adding the copolymer solution into the cassettes, the solution is only separated from the surrounding doubly distilled water via a semi-permeable membrane with a suitable molecular weight cut-off. This technique allows the water to diffuse into the dialysis cell to decrease the concentration of small particles with a M_w lower than the MWCO of the permeable membrane. This is achieved by diffusing out to sustain equilibrium of the overall dissolved particles without lowering the concentration of the copolymers inside the dialysis cell. To increase the efficiency the water is exchanged several times during the dialysis process which takes around 24 hours.

2.5 UV/Vis Spectroscopy

The basic concept behind UV/Vis spectroscopy is the law of Beer-Lambert which relates the absorption of light to the properties of the material through which the light is traveling.

1 Gel Permeation Chromatography
2 Polydispersity Index

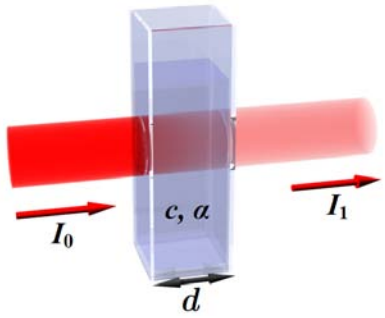

Figure 2.2: Beer-Lambert absorption of a beam of light as it travels through a cuvette.

The transmission T is a function of the intensity before I_0 and after I passing the sample. This can also be rewritten as a function of the absorbtion coefficient α and the path length d.

$$T = \frac{I}{I_0} = e^{-\alpha d} \tag{2.1}$$

In the experimental setup the absorbance A as a function of the wavelength λ is measured. Due to this the law of Beer-Lambert turns into its linear form:

$$A = -\ln\left(\frac{I}{I_0}\right) = \alpha d = \epsilon c d \tag{2.2}$$

The absorbtion coefficient α can be rewritten as the product of molar absorptivity ϵ and the concentration c of the absorbing species in the material.

2.5.1 Sample Preparation

Usually a series of dilutions in doubly distilled water until $1/256$ of the stock is prepared. These dilutions are then irradiated by UV light inside a quartz cuvette with a path length d of 1 cm. Since the absorbtion maximum of DNA lies at about 260 nm, we measured the absorbtion between 220 nm and 340 nm.

2.6 Fourier Transform Infrared Spectroscopy

FTIR[1] is an absorbance method which uses a spectrophotometer to examine the energy retained at each wavelength, typically between 4000 cm^{-1} and 670 cm^{-1}. Using FTIR measurements we are able to predict the configuration of the synthesized polymer [33]. Sample analysis was performed using a FTIR 8400 equipment from Shimadzu Scientific Equipments in the institute of inorganic chemistry. The measurements were performed using either air or *poly*(butadiene) to set the background prior to analysis. All spectra were recorded after 32 scans with a resolution of 2 cm^{-1}.

1 Fourier Transform Infrared Spectroscopy

2.7 Circular Dichroism Spectroscopy

CD[1] is a spectroscopic method in which the differential absorption of left- and right-handed circularly polarized light is monitored. With this information the determination of the structure of a macromolecule is possible, including the secondary structures of proteins and the conformation of nucleic acids [16]. CD is reported in units of absorbance or ellipticity. The ellipticity θ is measured in $mdeg$ and should be converted into molar ellipticity with the unit $deg \cdot cm^2 \cdot dmol^{-1}$.

2.8 Light Scattering

Light scattering is a powerful technique to characterize polymers [33]. Scattering results from the interaction of the electrons in the molecules with the oscillating electric field of radiation. The particle-wave duality of Einstein and de Broglie shows that light can interact with matter differently. In light scattering we measure a dilute solution of small particles at different concentrations and different angles.
If we measure light scattering we usually differentiate two major methods.

- SLS[2] is a technique used to get information about small particles such as radius of gyration, molecular weight and the second virial coefficient.
- DLS[3] measures the variation of scattered light with time. This gives information about the brownian motion of the molecules, characterized by their diffusion coefficient.

The light scattering setup used is consisting of a laser with a wavelength of $\lambda = 632.8$ nm, two mirrors, a sample holder and a photodetector which can be positioned in a range between 30° and 150°. The detector is connected to a computer which controls, records and analyzes the whole process.
In the next section the basic data analysis and some of the theory behind DLS and SLS is shown. We did not go into details since this was reported in my project thesis [24].

2.8.1 Charge Effects

Since we work with charged systems (i.e. DNA), also called polyelectrolytes, which are more difficult to handle both in water and in organic solvents due to long-range coulomb interactions between the scattering solute particles, these interactions may influence the experimental results in dynamic light scattering measurements [21, 23, 26, 27]. One common solution to this problem is to screen the disturbing coulomb interactions by adding salt. The addition of counter-ions then leads to electrolyte friction and the diffusion coefficient can strongly depend on the salt concentration [10]. Salt-free polyelectrolytes usually show a larger diffusion coefficient and therefore, the hydrodynamic radius becomes smaller.

1 Circular Dichroism
2 Static Light Scattering
3 Dynamic Light Scattering

2.8.2 Data Analysis

2.8.2.1 Static Light Scattering

In SLS we assume scattering from dilute solutions with comparatively small particles. This can be expressed by the following equation, where K is an optical constant, R the rayleigh ratio, c the concentration of the solute, M the molar mass, q the scattering vector, R_g the radius of gyration and A_2 the second viriral coefficient.

$$\frac{Kc}{R} = \frac{1}{M} \cdot \left(1 + \frac{q^2 R_g^2}{3}\right) + 2A_2 c \tag{2.3}$$

It gives the concentration and angle dependance of the quantity $\frac{Kc}{R}$. Thus the molar mass of the solute can be determined by extrapolation of experimental $\frac{Kc}{R}$ data to $c = 0$ and $q = 0$.
Since we are not only measuring at different concentrations but also at different angles, we also extrapolate to zero angle and can determine the weight average molecular mass M_w.

$$\left(\frac{Kc}{R_\theta}\right)_{\theta, c \to 0} = \frac{1}{M_w} \tag{2.4}$$

where R_θ is the measured value of R at the scattering angle θ (i.e. including the effects of size). From the weight average molecular mass we can also derive the radius of gyration R_g.

$$R_g = \sqrt{3 \cdot M_w \cdot S_{\frac{Kc}{R_\theta}}} \tag{2.5}$$

where $S_{\frac{Kc}{R_\theta}}$ is the average slope of $\frac{Kc}{R_\theta}$ versus the angle.

2.8.2.2 Dynamic Light Scattering

For exact data analysis the decay time τ in ms was monitored at every angle and concentration. By calculating $q = \frac{4\pi n}{\lambda} \cdot \sin(\frac{\theta}{2})$ using $\lambda = 6.328 \cdot 10^{-7}\ nm$ and $n = 1.332$, the average slope $D = \frac{1}{q^2 \tau}$ of every concentration could be calculated. D was then plotted and extrapolated to zero concentration by linear regression to get D_0. The hydrodynamic radius can be calculated according to equation 2.6.

$$R_h = \frac{k_B T}{6\pi \eta_0 D_0} \tag{2.6}$$

where $k_B = 1.381 \cdot 10^{-23}\ J \cdot K^{-1}$, $T = 293\ K$ and $\eta_0 = 1.0027 \cdot 10^{-3}\ Pa \cdot s$.

2.8.2.3 The ρ-Factor

The so-called ρ-factor is an experimental quantity derived from combining the particle size characteristics determined from static and dynamic light scattering measurements. The ρ-ratio provides an important indication of the scattering particle morphology, especially for comparatively small particles with sizes between 10 nm and 100 nm.
The ρ-factor is simply defined by the ratio between the radius of gyration R_g derived from SLS and the hydrodynamic radius R_h derived from DLS.

$$\rho = \frac{R_g}{R_h} \tag{2.7}$$

Theoretically calculated values of ρ-ratios for the most important particle morphologies [17] are shown in table 2.1.

Morphologies	*ρ-ratio*
Homogeneous Sphere	0.775
Hollow Sphere	1
Ellipsoid	0.775-4
Random Polymer Coil	1.505
Cylinder of Length l, Diameter D	$\frac{1}{\sqrt{3}} \cdot \ln\left(\frac{l}{D} - 0.5\right)$

Table 2.1: ρ-ratio for the most-typical particle morphologies

2.8.3 Sample Preparation

All the samples used for light scattering were dissolved or diluted in doubly distilled water. To get an accurate measurement, about six different concentrations were prepared. The stock solution between 1 $mg \cdot m\ell^{-1}$ and 2 $mg \cdot m\ell^{-1}$ was diluted to fractions of $1/2$, $1/4$, $1/5$ $1/8$ and $1/10$. Before measuring, the sample solution was centrifuged for 15 minutes at 4000 RPM[1] in order to sediment dust particles.

2.8.3.1 Solvent Displacement

Solvent Displacement is a technique to induce the self-assembly of amphiphilic block copolymers which are not soluble in water. The polymer is dissolved in an organic solvent like THF[2], in order to achieve a concentration of 40 $mg \cdot m\ell^{-1}$. 250 $\mu\ell$ of this solution were then added drop wise and very slowly to 5 $m\ell$ of doubly distilled water under stirring to obtain a 2 $mg \cdot m\ell^{-1}$ copolymer concentration. Adding the stock solution is displacing the THF by H_2O. The copolymers organize themselves driven by hydrophobic interactions and form self-assembled structures such as vesicles or micelles. This technique was applied only for PB-PEG since PB-siDNA self-assembles spontaneously in water.

1 Rounds per Minute
2 Tetrahydrofuran

2.8.4 Measurement

2.8.4.1 Dynamic Light Scattering

For DLS it is not necessary to measure a standard or a blank, also the concentration has not to be known absolutely but relatively. The samples with different concentrations were measured at different angles between 30° and 150° in steps of 20° for 5 minutes each.

2.8.4.2 Static Light Scattering

Since the sample is placed in a toluene bath, the scattering of a toluene sample has to be measured to aligne the setup and as a standard for the software. Subsequently, the data for the solvent as a blank sample was recorded. Finally, the samples with different concentrations were measured at different angles between 30° and 150° in steps of 10° for 30 seconds each. Note that the software requires the concentration as well as the refractive index increment of the solute in order to start a measurement.

2.8.4.3 Specific Refractive Index Increment

The refractive index increment was measured within concentrations between 0.1 $mg \cdot m\ell^{-1}$ and 1 $mg \cdot m\ell^{-1}$. The sample was placed in a two-cell chamber divided by a 45°-glass wall with the solvent in the other chamber. First, the solvent was measured as reference and then the samples were exchanged into one of the two chambers of the cell with increasing concentration. The computer program provides the $n - n_{ref}$-values and the refractive index increment can be determined by the slope of a linear regression of the function $(n - n_{ref})\,(c)$.

2.9 Transmission Electron Microscopy

TEM[1] is a microscopy technique whereby a beam of electrons is transmitted through an ultra thin specimen, interacting with the specimen as they pass through [25]. An image is formed from the interaction of the electrons transmitted through the specimen. The maximum resolution d is theoretically dependent on the wavelength λ and the numerical aperture NA of the system (see equation 3.2).

$$d = \frac{\lambda}{2 \cdot n \cdot \sin\alpha} \approx \frac{\lambda}{2 \cdot NA} \tag{2.8}$$

Compared to light microscopes with wavelengths between 400 nm and 700 nm a TEM is able to achieve a much higher resolution due to the much smaller de Broglie wavelength of electrons. With high resolution TEM it is possible to see atoms which are separated from each other only 0.78 Å, this at a magnification of 50 million times [1].

1 Transmission Electron Microscopy

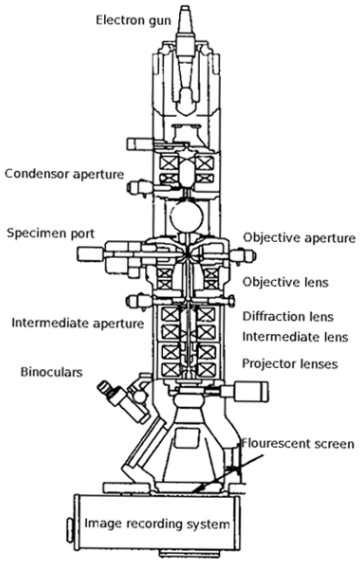

Figure 2.3: Scheme of a typical transmission electron microscope. Note that the sample is placed in between the electron beam.

The setup of a TEM is very similar to a light microscope (see figure 2.3). It consists of an emission source, which is a tungsten filament in our case, this part is also called electron gun. By connecting this filament to an HV[1] source the gun will, given sufficient current, begin to emit electrons into the vacuum. Once extracted, the upper lenses of the TEM allow for the formation of the electron probe to the desired size and location for subsequent interaction with the sample. Typically a TEM consists of three stages of lensing. The stages are the condenser lenses, the objective lenses, and the projector lenses. The condenser lenses are responsible for primary beam formation, whilst the objective lenses focus the beam down onto the sample itself. The projector lenses are used to expand the beam onto the phosphor screen or the other imaging device.
Imaging systems in a TEM consist of a phosphor screen for direct observation by the operator. Optionally, an image recording system can be inserted into the beam path as required.

2.9.1 Sample Preparation

There are several methods to prepare the samples for TEM depending on the sample thickness. It is necessary to have a very thin film on the grid, which is exposed to the electrons, in order to let them through the sample. We used negative staining to intensify the contrast. Therefore the samples were treated with uranyl acetate, which contains heavy, radioactive atoms to scatter the electrons better. Negative staining is often used for imaging biological materials.

1 High Voltage

2.10 Atomic Force Microscopy

AFM[1] is one of the most powerful tools for determining the surface topography of native bio-molecules at subnanometer resolution and was invented by Binnig, Quate and Gerber in 1986 [3].
Tapping mode AFM analysis of the samples was performed using a Nanoscope IIIa D3000 from Digital Instruments with silicon cantilever from Veeco (phosphorous doped Si, $f = 272 - 318\ kHz$, $k = 20 - 80\ N \cdot m^{-1}$). Different areas of the samples were imaged. All experiments were done in air at room temperature.

2.10.1 Sample Preparation

Polished silicon wafers were cut into pieces of approximately $1 \times 1\ cm^2$. To clean the surface we used chloroform rinsing as a water-free non-destructive method. The silicon wafers were cleaned 3 times ultrasonically in chloroform for 15 minutes, rinsed with chloroform 3 times. To reveal hydroxyl groups onto the surface of some samples, they were activated in a UV/ozone chamber (UVO-cleaner, model 42-220, Jelight Company Inc. USA) during 15 minutes. For each sample we used 20 $\mu\ell$ of 1 $mg \cdot m\ell^{-1}$ PB-siDNA in doubly distilled water .

2.11 Scanning Electron Microscopy

SEM[2] is a special form of electron microscopy. The sample is irradiated by an electron beam and the dislodged secondary electrons are attracted by a positively charged grid, where they are translated into a signal. By scanning the surface of the sample, an image is generated.
All measurements were performed on a Hitachi S-4800 SEM with a cold field emission electron source in the *Zentrum Mikroskopie der Universität Basel*. In order to have an electrically conducting surface all samples were sputtered with a platinum layer of 5 nm.

2.12 Confocal Laser Scanning Microscopy

CLSM[3] is a special line of microscopes [6]. We used a LSM 510 Meta produced by Carl Zeiss AG, Germany which is an inverted confocal laser microscope. With this technique we are able to record transmission as well as fluorescence micrograph images of the specimen at the same time. The fluorescence signal from Alexa488-labeled copolymers, was registered upon emission at 488 nm wavelength with 505 nm to 550 nm emission filters (green channel) using a 40x C-Apochromat water-immersion objective.

1 Atomic Force Microscopy
2 Scanning Electron Microscopy
3 Confocal Laser Scanning Microscopy

2.13 THP-1 Cells

The cell line used for the growth experiments and to test the cytotoxicity of PB-siDNA was the THP-1 cell line, a human acute monocytic leukemia cell line [31] obtained from the university hospital in Basel. The THP-1 cell line was cultured in RPMI 1640 medium (GIBCO, Invitrogen) containing 1 $m\ell$ non-essential amino-acids, 1 $m\ell$ penicillin-streptacide, 1 $m\ell$ sodium pyruvate, 100 $\mu\ell$ of β-mercaptoethanol and 10% FCS per 100 $m\ell$ medium, in a 5% CO_2 humidified atmosphere at 37 $°C$. After reaching confluence which takes about a week, cells were passaged in a split ratio of 1:5 and 1:10. After a 24 hours recovery period, THP-1 cells were incubated with various concentrations of self-assembled PB-siDNA or PB-PEG in doubly distilled water (see section 3.3). All experiments were performed in 12-well plates with cells between passages 15 and 19.

CHAPTER 3

Results and Discussion

3.1 PB_{2000}-siDNA

Before using PB-siDNA for cell experiments we have to ensure the linking of the two blocks as well as characterize the self-assembled structure. For that purpose we performed several chemical and physical characterizations.

3.1.1 Characterization of the Chemical Structure

3.1.1.1 Fourier Transform Infrared Spectroscopy

As described in section 2.6, FTIR can predict the structural conformation of a polymer. In our case this method was mainly used to confirm the linkage of the two blocks via the amide bond. For that reason spectra of the nucleotide-based block copolymer were recorded using air or PB as background to see if the bands for PB as well as the ones for oligonucleotides are present. The comparison of these two measurements confirms the presence of PB. To ensure that the coupling of the two blocks took place, a band at around 1530 cm^{-1} for the NH-C=O vibration must be seen [4].
Although the guanosine has as well an amide function in its structure we can neglect it. This follows from the fact that the guanosine is a lactam which does not appear in FTIR spectra but rather corresponds to aromatic resonance structures. This leads to the conclusion that the peak at 1530 cm^{-1} is a very important criteria for the linking process even if guanosine is present. In figure 3.1 the peak at 1530 cm^{-1} can be observed as well as the other peaks defining the oligonucleotides present in the copolymer. This indicates and confirms the successful coupling reaction.

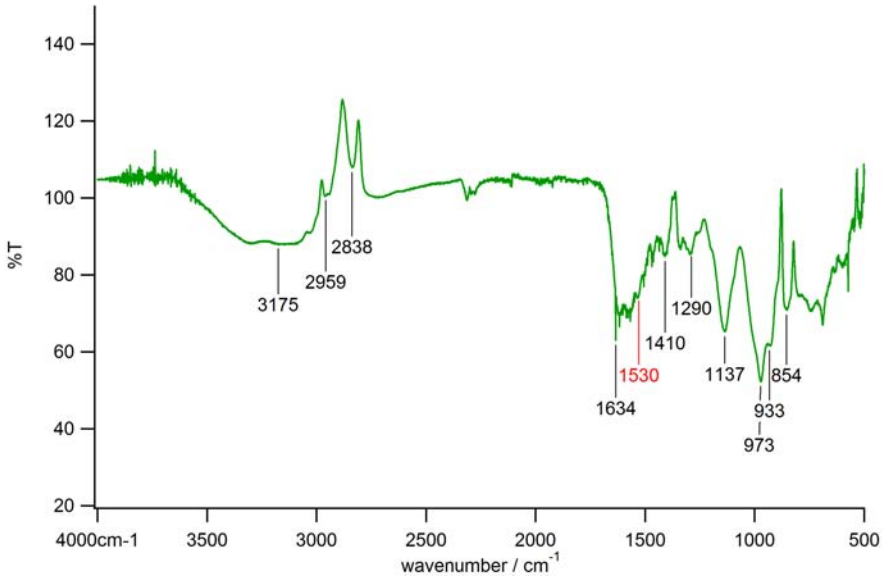

Figure 3.1: FTIR spectrum of PB-siDNA with PB background. Indicated in red is the absorbance band of NH-C=O which confirms the successful coupling of the two different blocks.

In table 3.1 the major peaks defining our copolymer are summarized. The bands at 1530 cm^{-1} and 1634 cm^{-1} are defining the amide bond whereas the bands between 1137 cm^{-1} and 854 cm^{-1} confirm the presence of the sugar backbone from the siDNA.

wavenumber [cm^{-1}]	*vibration*
1634	$\nu_{C=O}$ (for secondary amides)
1530	δ_{N-H}
1137	$\nu_{P=O}$ in (R-O)$_2$-PO$_2$ upper band
973	$\nu_{P=O}$ in (R-O)$_2$-PO$_2$ lower band
933	ν_{P-O} in (R-O)$_2$-PO$_2$ upper band
854	ν_{P-O} in (R-O)$_2$-PO$_2$ lower band

Table 3.1: FTIR vibration bands an their corresponding wavenumber for PB-siDNA

3.1.1.2 Circular Dichroism Spectroscopy

A CD spectra of our copolymer (0.15 $mg \cdot m\ell^{-1}$ in doubly distilled water) was recorded in comparison to PIB-A_5G_7, another copolymer synthesized in our group. As figure 3.2 shows, the spectrum of PB-siDNA is not similar but comparable with the one of PIB-A_5G_7. This is what we estimate due to the fact that they do not have the same DNA sequence and length. One effect of different DNA sequences is a shift in wavelenth which can be observed in figure 3.2. Still we see that the shape of the CD spectra looks as expected for DNA structures in its A-form with its chiral centers and the right handed helix [16]. This further confirms the presence of DNA with a secondary structure. Note that our sequence is not self-hybridizing as assessed with OligoCalc [14].

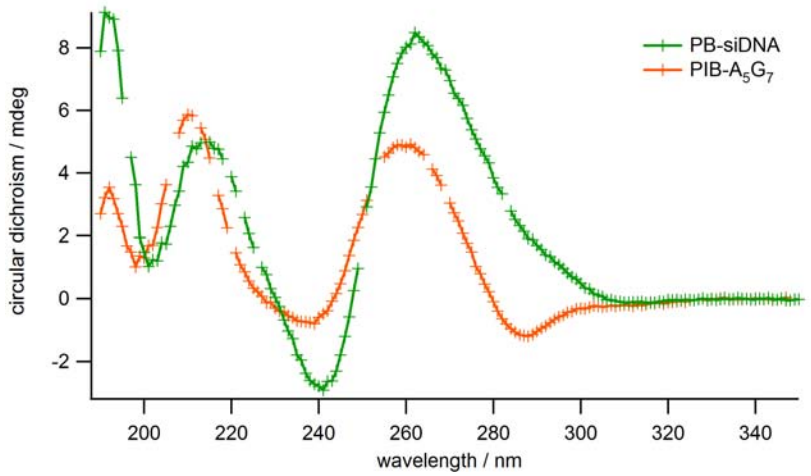

Figure 3.2: CD spectrum of PB-siDNA in comparison to the one of PIB-A_5G_7.

3.1.2 Characterization of the Self-Assembled Structure

3.1.2.1 UV/Vis Spectroscopy

UV/Vis spectroscopy was performed with dilution of $^1/_8$ to $^1/_{256}$ from a stock solution of 1 $mg \cdot m\ell^{-1}$ of PB-siDNA in doubly distilled, filtered water. The absorbtion maximum for DNA lies at around 260 nm depending on the composition of the different nucleotides in the measured sequence [5]. The measurement (see figure 3.3) results in an absorbtion maximum at 256 nm. If we compare this with generated data of our sequence (see figure 3.4) we see the same absorbtion maximum [30]. This confirms the presence of our oligonucleotide sequence.

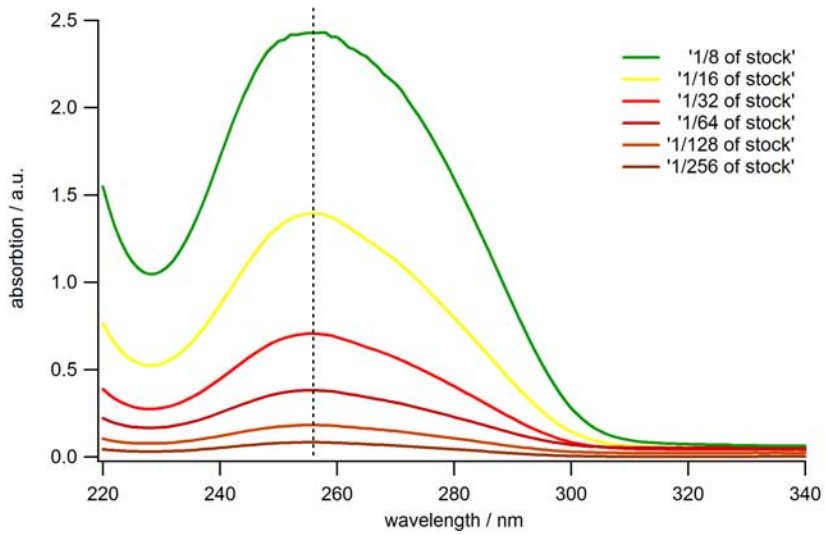

Figure 3.3: UV/Vis absorbtion spectrum of PB-siDNA shows an absorbtion maximum at 256 nm.

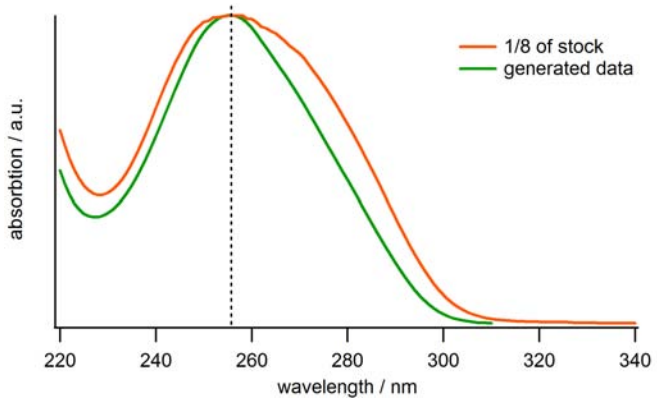

Figure 3.4: UV/Vis absorbtion spectrum of PB-siDNA compared to data specifically generated for our sequence by the IDT Biophysics website [30]. Both spectra show an absorbtion maximum at 256 nm. This confirms the presence of bound nucleotides in our copolymer.

Using OligoCalc a Biotool which calculates properties of oligonucleotides based on their nucleotide sequence and UV/Vis absorbtion maximum [14], we could estimate the concentration as well as the mass of siDNA present in our solution. These results are listed in table 3.2. Note that the concentration can also be applied to our copolymer but not the mass which counts only for the siDNA itself.

Dilution	*Max. Absorbtion*	*Conc [μmol]*	*Mass [μg]*
$^1/_8$	2.4313	9.580	63.1
$^1/_{16}$	1.3943	5.494	36.2
$^1/_{32}$	0.7064	2.783	18.3
$^1/_{64}$	0.3819	1.505	9.9
$^1/_{128}$	0.1824	0.719	4.7
$^1/_{254}$	0.0833	0.328	2.2

Table 3.2: UV/Vis absorbtion maxima, concentrations and masses for PB-siDNA

3.1.2.2 Scanning Electron Microscopy

To confirm the self-assembly of the polymers in solution, samples of PB-siDNA have been analyzed with SEM.

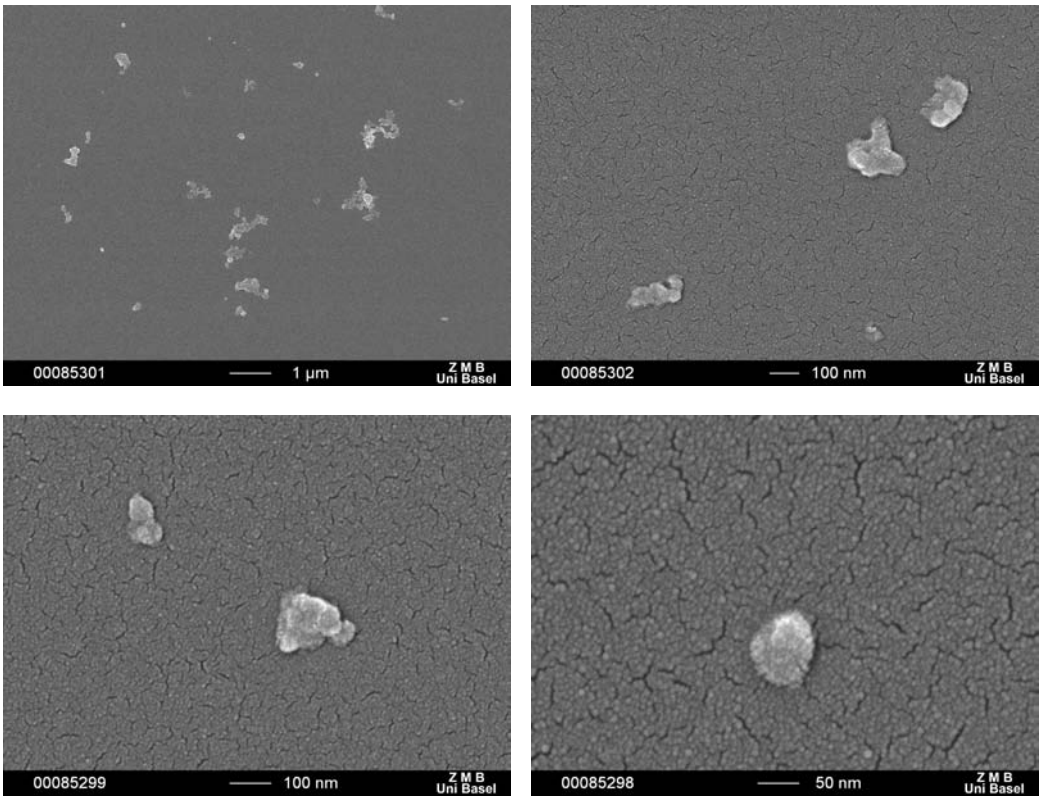

Figure 3.5: SEM pictures of PB-siDNA at different magnifications.

Samples for SEM were prepared using the method described in section 2.11 and 2.10.1. The results, shown in figure 3.5, are not very easy to interpret, because the copolymer was forming aggregates. Further, the sputtering of the sample with platinum was making some problems due to the fact that the machine was not working properly. The little dots and cracks are coming from this sputtered surface and we are not sure how much the samples were affected by this process.
Despite all that, we can make some assumptions regarding the polymer size and shape. From the lower right image we can estimate a radius of approximately 30 *nm* for one self-assembled structure. Due to this we can assume vesicular structure but this cannot be confirmed by the picture itself, it is more an estimation from experience.

3.1.2.3 Atomic Force Microscopy

Since the SEM pictures were not very meaningful, we decided to image the self-assembled PB-siDNA also with tapping mode AFM. The samples were prepared as described in section 2.10.1.

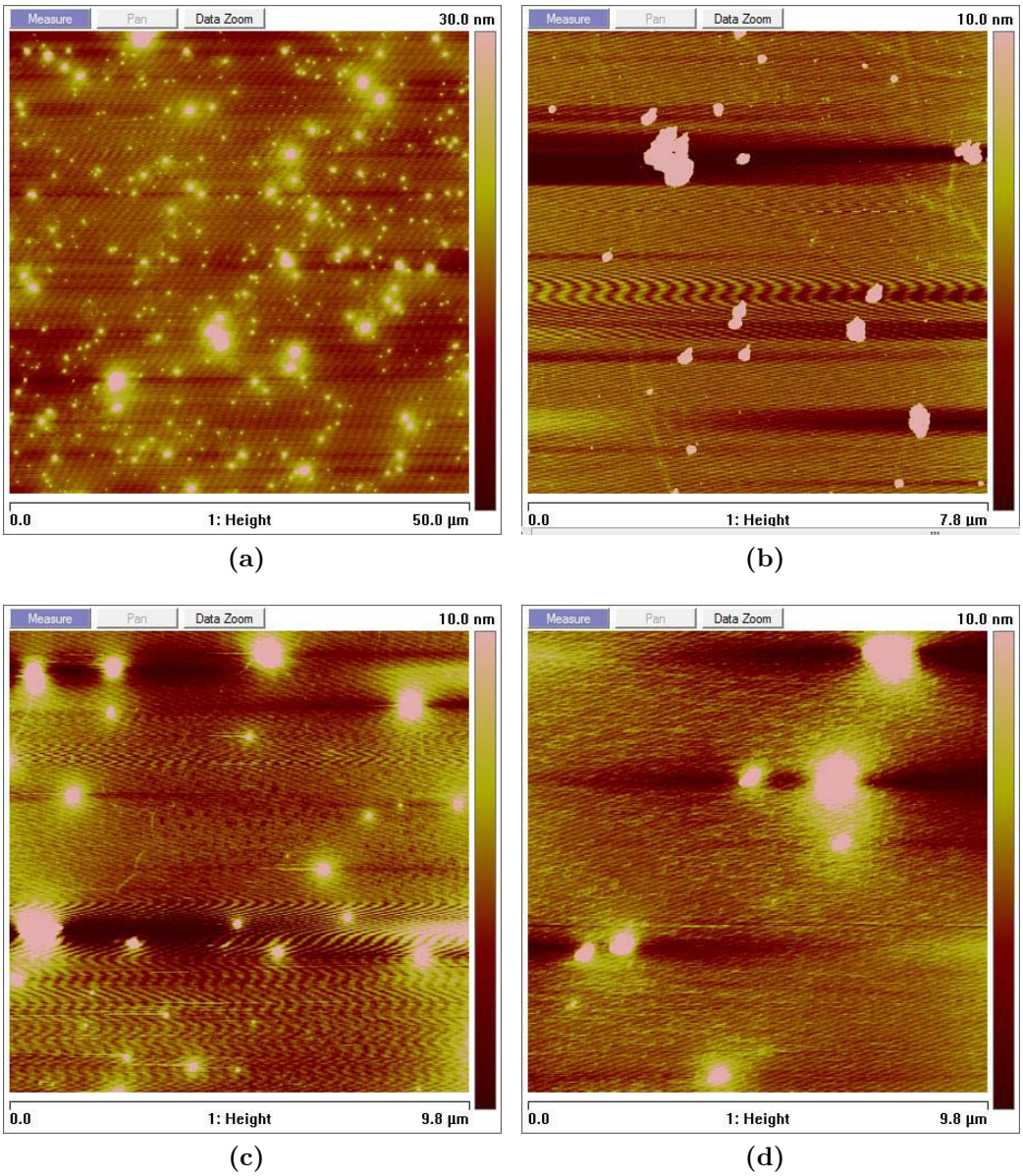

Figure 3.6: AFM height images of PB-siDNA on silicon and mica. (a) shows PB-siDNA on SiO_2 substrate, (b) shows PB-siDNA on SiO_2 substrate after rinsing with H_2O, (c) shows PB-siDNA on SiO_2 substrate which was activated with UV and (d) shows PB-siDNA on mica.

In Figure 3.6, the self-assembled PB-siDNA displays distinct morphologies of spherical structures regardless of substrate used.

Looking at the phase picture 3.7, we can make better assumptions on the structure. Phase imaging goes beyond simple topographical mapping and can detect variations in composition, adhesion, friction, viscoelasticity, and perhaps other properties. Applications include identification of contaminants, mapping of different components in composite materials, and differentiating regions of high and low surface adhesion or hardness.

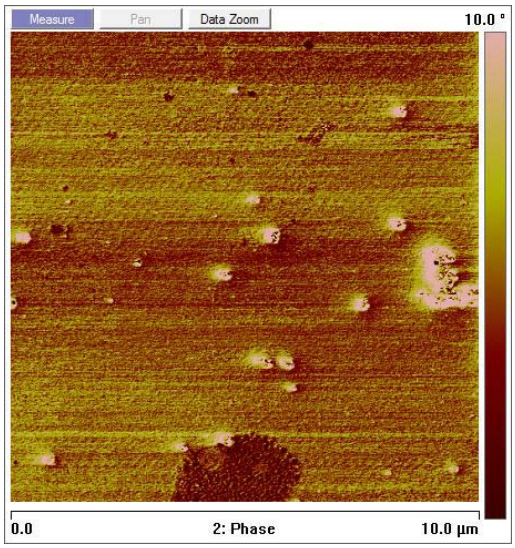

Figure 3.7: AFM phase images of PB-siDNA on SiO_2 substrate. Phase information leads to the conclusion that the self-assembled structures are vesicles.

Image 3.7 leads to the conclusion that we have self-assembled vesicles due to the fact that we can see a change in phase if we scan over an individual spherical structure which corresponds to the cavity inside the vesicle.
Further, we can estimate the size of the vesicles by looking at a section of the height image. In figure 3.7 two sections through self-assembled structures are shown.

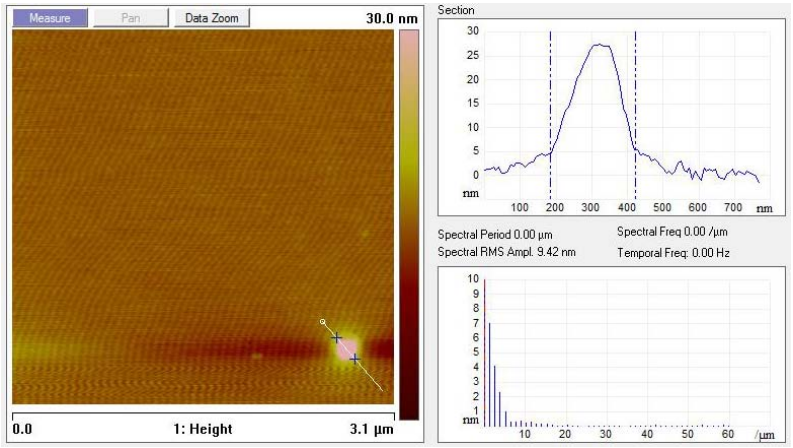

(a)

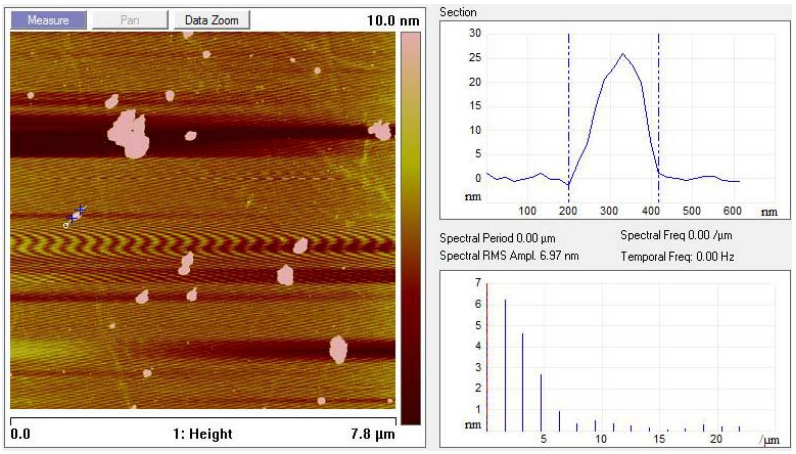

(b)

Figure 3.7: Sections of AFM height images with PB-siDNA (a) shows PB-siDNA on SiO_2 substrate and (b) shows PB-siDNA on SiO_2 substrate after rinsing with H_2O.

The sections show an elliptic shape of the self-assembled structure. Since the vesicle is adhered onto a surface we can assume deformation of the shape due to the deposition. Both sections indicate a size of $a = 200\ nm$ in length and $b = 25\ nm$ in height. With these two values we can calculate the circumference of the ellipse by the equation of Ramanujan.

$$C \cong \left(\frac{a}{2} + \frac{b}{2}\right) \cdot \pi \cdot \left(1 + \frac{3\lambda^2}{10 + \sqrt{4 - 3\lambda^2}}\right) \tag{3.1}$$

where $\lambda = \frac{a-b}{a+b}$. This leads to a circumference of 410 nm which further yields in a radius of approximately 65 nm for a hollow sphere.

3.1.2.4 Dynamic Light Scattering

DLS was performed according to section 2.8 and we induced self-assembly of PB-siDNA by dissolving in doubly distilled water. The extrapolation to zero concentration shown in figure 3.8 yields in the diffusion coefficient D_0. Due to the extrapolation to zero concentration the concentration has not to be known absolutely but relatively.

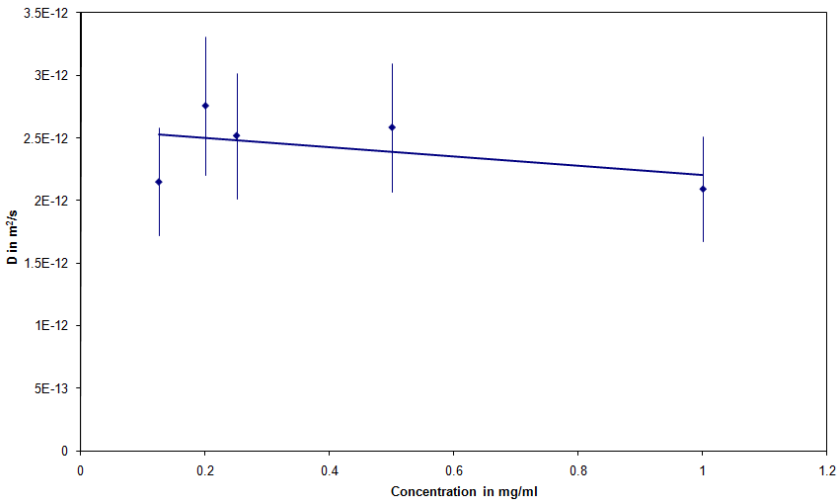

Figure 3.8: Extrapolation of D_0 to zero concentration for PB-siDNA. The extrapolation yields in a value of $2.42 \cdot 10^{-12}\ m^2/s$ for D_0.

The value of $2.42 \cdot 10^{-12}\ m^2/s$ for D_0 and equation 2.6 allows the calculation of the hydrodynamic radius R_h of $88 \pm 11\ nm$ for an individual vesicle.

$R_h \pm \Delta R_h$ *[nm]*	ΔR_h *[%]*
88 ± 11	12

Table 3.3: DLS results for PB-siDNA

A comparison of the hydrodynamic radius to other types of radii can be shown using lysozyme as an example (figure 3.9). R_h is the hydrodynamic radius, R_g the radius of gyration, R_M is the equivalent radius of a sphere with the same mass and particle specific volume as lysozyme, and R_R is the radius established by rotating the protein about the geometric center.

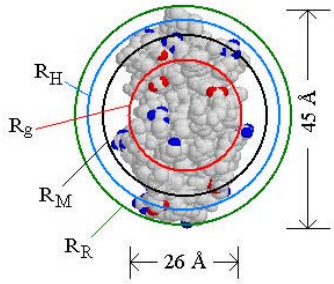

Figure 3.9: Comparison of hydrodynamic radius R_h to other radii for lysozyme.

From this figure we can see very clearly, that R_h is expected to be bigger than R_M, the hypothetical radius for a hard sphere because it includes both solvent (*hydro*) and shape (*dynamic*) effects. Further, we have to take the effect of electrostatic interactions for DLS into account which tend to result in a smaller R_h (see section 2.8.1). Thus, the radius gained from AFM (R_M) can be compared with the one from DLS (R_h).

3.2 PB_{2000}-PEG

This polymer is consisting out of a *poly*(butadiene) and a *poly*(ethylene-glycol) block (PEG is the name used by biologists whereas the chemists call it PEO[1]. We will stick to the biologists nomenclature due to the fact that we use it for cell experiments). It was produced by the group of Axel Müller in Bayreuth. These PB-PEG polymers are highly pure and already briefly analyzed. We decided to characterize it further in order to use it as a biologically inert system for the cell experiments (see section 3.3).
The group of Axel Müller already delivered some information about the polymer: According to their calculations the copolymer has a M_n of 6100 $g \cdot mol^{-1}$ with 40% PEG and a PDI of 1.06. Due to that we can say that the *poly*(butadiene) part has the same length as our PB_{2000} part used for the synthesis of PB-siDNA (see section 2.1). To confirm the molecular weight as well as the PDI, we performed GPC and to make estimations about the self-assembled structure we performed DLS/SLS and TEM.

3.2.1 Characterization of the Chemical Structure

3.2.1.1 Gel Permeation Chromatography

As explained in section 2.3.1, GPC is used to calculate the different molecular weights and the PDI. Self-assembly was induced by the solvent displacement method (see section 2.8.3). For GPC it was dissolved in chloroform and measured using *poly*(butadiene) as a standard (for the calibration data of PB in chloroform see appendix A).

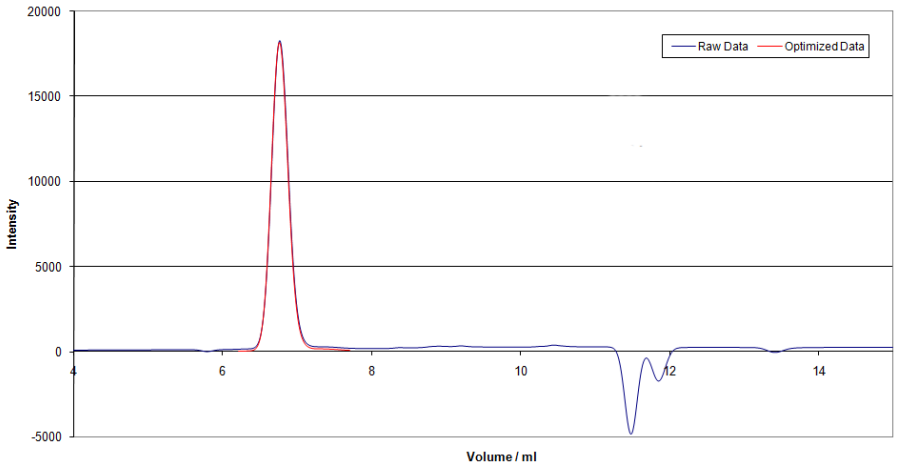

Figure 3.10: GPC data for PB-PEG with the optimized data shown in red.

Due to the optimized data gained from fitting the GPC raw data we can determine the molecular weight and the PDI.

1 *Poly*(Ethylene-Oxide)

M_n [g/mol]	M_w [g/mol]	PDI
6490.94	6717.16	1.03

Table 3.4: GPC results for PB-PEG with PB standard

The characterization made by the group of Axel Müller resulted in a M_n of 6100 $g \cdot mol^{-1}$ and a PDI of 1.06 which is confirmed with our result although it differs a bit. One of the reasons is that it is not very easy to find an appropriate calibration standard for PB-PEG. Working with PEG standards give us other results than with PB standards.

3.2.2 Characterization of the Self-Assembled Structure

3.2.2.1 Dynamic Light Scattering

Preparation of the samples for DLS was performed using the solvent displacement method (see section 2.8.3). Figure 3.11 shows the extrapolation to zero concentration which yields the diffusion coefficient D_0. Due to the extrapolation to zero concentration the concentration has not to be known absolutely but relatively.

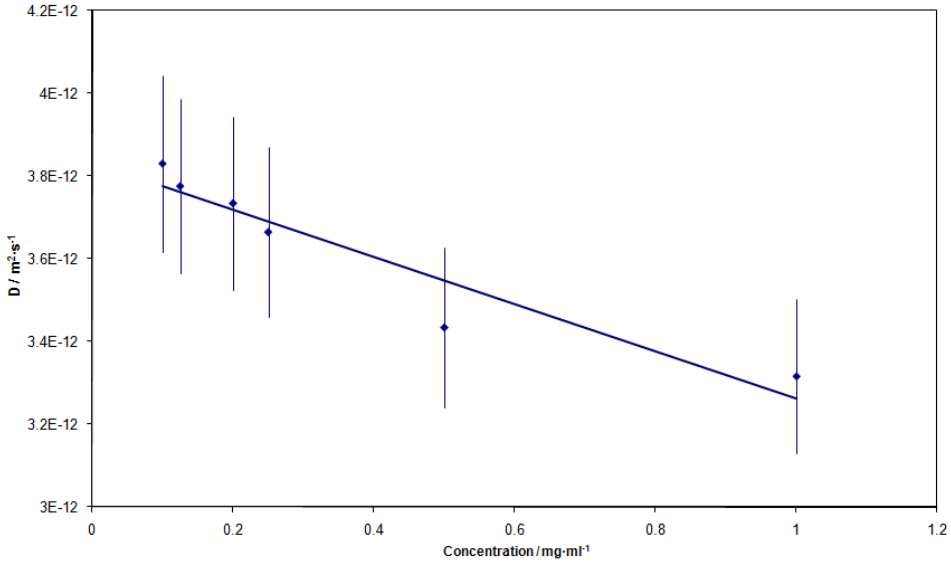

Figure 3.11: Extrapolation of D_0 to zero concentration for PB-PEG. The extrapolation yields in a value of $3.63 \cdot 10^{-12}\ m^2 \cdot s^{-1}$ for D_0.

The value of $3.63 \cdot 10^{-12}\ m^2 \cdot s^{-1}$ for D_0 with equation 2.6 allows the calculation of the hydrodynamic radius R_h.

$R_h \pm \Delta R_h$ [nm]	ΔR_h [%]
59 ± 4	6

Table 3.5: DLS results for PB-PEG

3.2.2.2 Static Light Scattering

Preparation of the samples for SLS was performed using the solvent displacement method (see section 2.8.3). Before measuring SLS the specific refractive index increment of PB-PEG was measured (see section 2.8.4.3).

$\frac{dn}{dc} \pm \Delta\frac{dn}{dc}$ $[m\ell \cdot g^{-1}]$	$\Delta\frac{dn}{dc}$ [%]
0.91 ± 0.02	2

Table 3.6: Refractive index increment for PB-PEG

Figure 3.12 shows the extrapolation of $\frac{Kc}{R_\theta}$ to zero concentration which yields the weight average molecular mass M_w of the self-assembled structure.

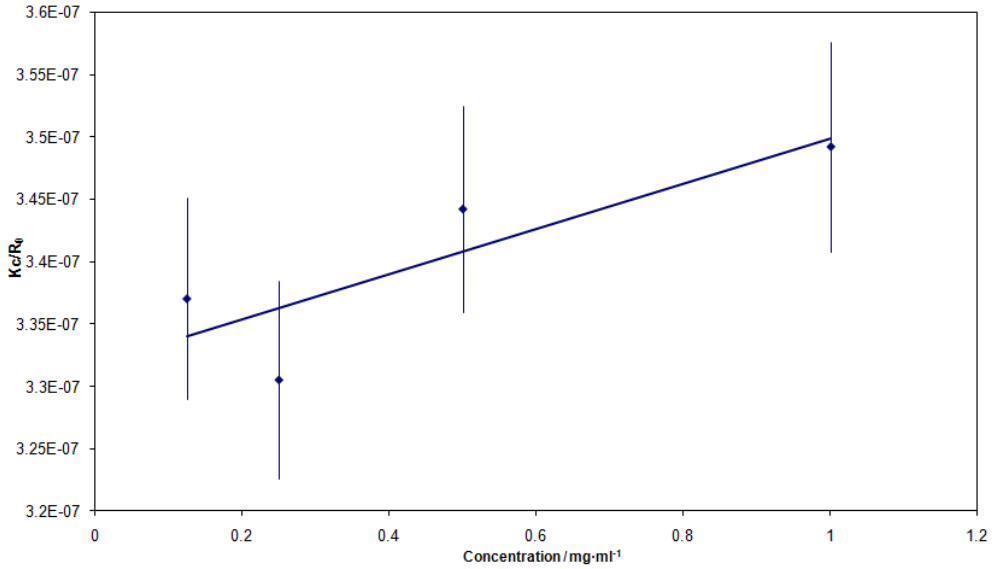

Figure 3.12: Extrapolation of $\frac{Kc}{R_\theta}$ to zero concentration for PB-PEG.

The value of 3013923 $g \cdot mol^{-1}$ for M_w with equation 2.5 allows the calculation of the radius of gyration R_g.

$R_g \pm \Delta R_g$ [nm]	ΔR_g [%]
80 ± 2	3

Table 3.7: SLS results for PB-PEG

Having both, the radius of gyration and the hydrodynamic radius we are able to compare them and make assumption about the morphology of PB-PEG via calculating the ρ-factor.

3.2.2.3 ρ-factor

The ρ-value for PB-PEG is calculated with equation 2.7.

$$\rho = \frac{R_g}{R_h} = 1.35 \tag{3.2}$$

According to table 2.1 a hollow sphere has a ratio of 1. In the case of PB-PEG in doubly distilled water the ρ-ratio indicates that the shape is a little elliptic. Also it could be an effect of a polydisperse sample but a PDI of 1.03 (see table 3.4) neglects that. TEM images of the self-assembled structure (see figure 3.13) confirm the presence of hollow spheres.

3.2.2.4 Transmission Electron Microscopy

For PB-PEG we performed TEM to confirm the presence of self-assembled vesicles. The samples were prepared using the method described in section 2.9.1 and are shown in figure 3.13.

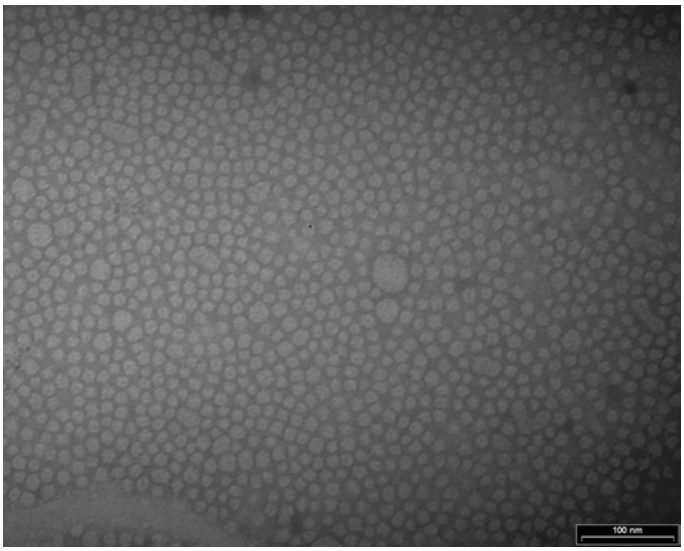

Figure 3.13: TEM pictures of PB-PEG.

The image verifies the formation of self-assembled vesicles but since they are crowded we cannot make reliable assumption about the asymmetry of the shape.

3.3 Preliminary Biological Assays

Once we characterized PB-siDNA, in order to develop applications for biological systems it is necessary to study whether this polymer-modified oligonucleotide sequence induces any toxic effects. Since we used a DNA sequence which plays a role in the back-fusion process involved in viral capsid release [19], we hope to see some effects on the growth of the cells as well as in the cytotoxicity assays. To compare the influence of PB-siDNA on cells with a biologically inert system, we used PB-PEG which was used for cell studies before [18]. For all the cell experiments we used the THP-1 human acute monocytic leukemia cancer cell line with distinct monocytic markers [31]. These well studied cells are used to test leukemia cell lines in immunocytochemical analysis of protein-protein interaction, and immunohistochemistry. Further, they can be differentiated into macrophage-like cells which is especially interesting for internalization studies [31].

3.3.1 Growth Study

First, a simple growth study of THP-1 cells with additives was performed (see section 2.13). To a 4 $m\ell$ colony with starting concentration of 325000 $cells \cdot m\ell^{-1}$ we added 500 nM PB-siDNA or 500 nM PB-PEG respectively in 100 $\mu\ell$ doubly distilled water. As a control we used a 4 $m\ell$ colony with starting concentration of 325000 $cells \cdot m\ell^{-1}$ and added 100 $\mu\ell$ doubly distilled water. The cells were counted every 24 hours for 5 days using the Neubauer improved assay. The experiments were prepared in two wells each and counted twice per well and day in order to evaluate the accuracy and reproducibility. In figure 3.14 we see the cell growth of THP-1 over a time frame of 120 hours.

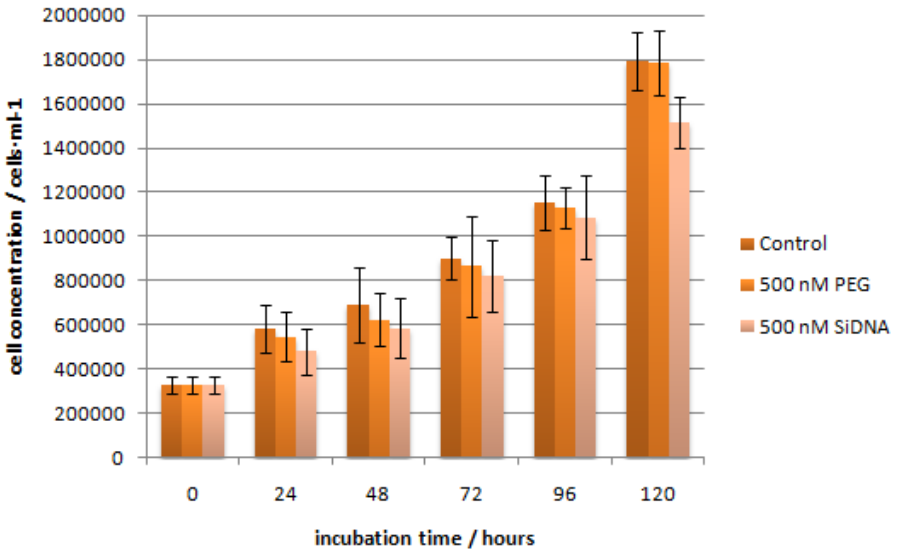

Figure 3.14: THP-1 cell growth study with 500 nM PB-siDNA and 500 nM PB-PEG as additives. The concentration of cells with PB-siDNA as an additive is increasing slower compared to the control and to PB-PEG.

The concentration of cells with PB-siDNA as an additive is increasing slower compared to the ones with PB-PEG and to the control, this could indicate a certain effect from the cytotoxicity of PB-siDNA. Each data point is the mean of the four different values gained from the experiment, the error bars were calculated using standard deviation. In order to have a better overview we repeated the calculation at four different concentrations with both copolymers PB-siDNA and PB-PEG (see figure 3.15).

3.3.2 Bio-Compatibility Assays

The cytotoxicity of PB-siDNA and PB-PEG was evaluated *in vitro*. For that purpose THP-1 cells were incubated with medium containing vesicles at four different concentration (2 μM, 1 μM, 500 nM and 100 nM). We used a total of 18 wells to determine the cytotoxicity of the two copolymers, two for each concentration of either copolymer and two for the control. Each well contained 4 $m\ell$ cells in medium with a starting concentration of $328250 \pm 39400\ cells \cdot m\ell^{-1}$. To each well we added 100 $\mu\ell$ of additive in doubly distilled water with the corresponding concentration. To ensure that the control has the same starting conditions, we added 100 $\mu\ell$ of doubly distilled water without additive.
The cytotoxicity of the polymer-modified oligonucleotides was determined by a viability quantitative assay. In this assay, one calculates the relation between the total number of cells and the number of non-viable ones. The comparison with a control sample without additive will provide a good indication of the cytotoxicity of the tested material. In order to differ between dead and alive cells, trypan blue, a common dye which permeates the membrane of dead cells, turning them blue, was used.
Each well was counted twice every 24 hours for five days using the Neubauer improved test. This leads to a total of 2×2 independent values for each concentration and additive per day. From these four different values the error was calculated using standard deviation.

Total Cells [$Mio\,cells/m\ell$]	*Viable Cells* [$Mio\,cells/m\ell$]	*Non-Viable Cells* [$Mio\,cells/m\ell$]	*Non-Viable Cells* [%]	*Error* [%]
1.842	1.793	0.049	3	0.5

Table 3.8: Cytotoxicity results for the control

PB-siDNA Conc [μM]	*Total Cells* [$Mio\,cells/m\ell$]	*Viable Cells* [$Mio\,cells/m\ell$]	*Non-Viable Cells* [$Mio\,cells/m\ell$]	*Non-Viable Cells* [%]	*Error* [%]
2	1.626	1.552	0.074	5	0.4
1	1.574	1.496	0.078	5	0.6
0.5	1.515	1.439	0.076	5	0.6
0.1	1.367	1.298	0.069	5	0.5

Table 3.9: Cytotoxicity results for PB-siDNA

PB-PEG Conc [μM]	Total Cells [$Mio\,cells/m\ell$]	Viable Cells [$Mio\,cells/m\ell$]	Non-Viable Cells [$Mio\,cells/m\ell$]	Non-Viable Cells [%]	Error [%]
2	1.813	1.741	0.072	4	0.9
1	1.833	1.762	0.071	4	0.8
0.5	1.773	1.703	0.070	4	0.6
0.1	1.825	1.763	0.062	3.5	0.7

Table 3.10: Cytotoxicity results for PB-PEG

The results shown in tables 3.8, 3.9 and 3.10 are all data gained after 120 hours of incubation with the corresponding additives. One can conclude that these experiments evidenced a very low cytotoxicity for both copolymers since no visible increase in the percentage of non-viable cells can be perceived.
To have a closer look at the concentration dependance, we performed an additional growth study of THP-1 cells which shows the amount of viable cells present in the wells after 120 hours of incubation. The data can be seen in figure 3.15 (for raw data see appendix B).

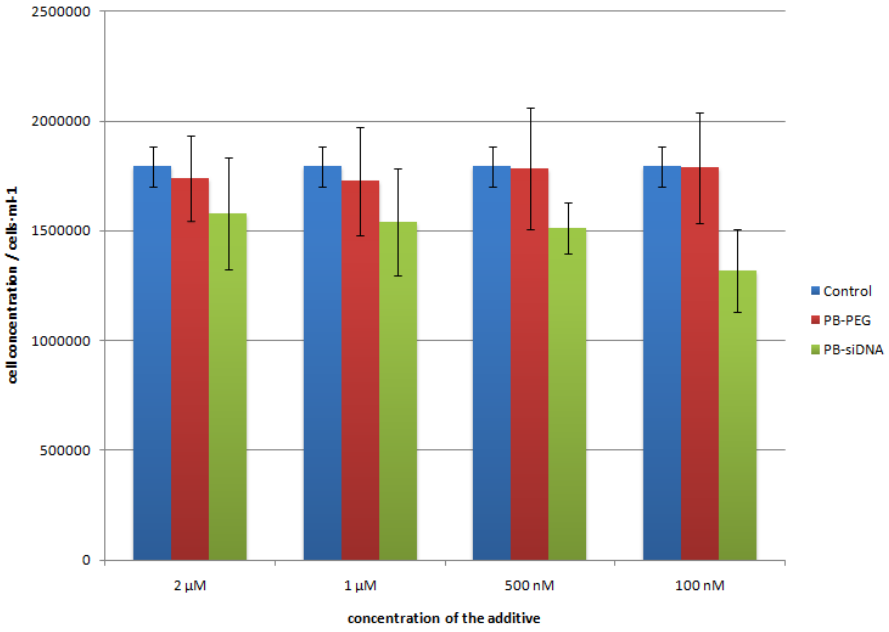

Figure 3.15: THP-1 cell growth study with PB-siDNA and PB-PEG as additives in different concentrations. The concentration of cells with PB-PEG was not effected much whereas the cell concentration with PB-siDNA is decreasing with increasing additive concentration.

The observation that the PB-siDNA is reducing the cell growth of THP-1 cancer cells without being toxic is very interesting. If the self-assembled PB-siDNA is only targeting cancer cells and has no toxic effect on other (i.e. healthy) cells lines, one could think of using them for cancer therapy. Further experiments (i.e. with other cell lines) are still necessary in order to clarify if only the growth of cancer cells is affected.

3.3.3 Internalization Studies

Since the biologically active PB-siDNA does not induce cell death but reduces the growth, it is important to understand how it influences the cells. For this purpose studies to assess if the self-assembled structures were internalized by the THP-1 cells, were performed. This can indicate reasons for the reduced cell growth induced by PB-siDNA but is also an important feature if one wishes to develop a carrier system. In order to resolve this point, further studies with THP-1 cells were performed to determine if PB-siDNA could be uptaken. THP-1 cells were chosen due to their ability to differentiate into macrophages which show a high internalization ability [31].
Figure 3.16 shows that after incubation some structures can be observed inside the cells. These structures are probably the result of the internalization process, like phagocytosis or a recognition-driven uptake, induced by the siDNA sequence. In Figure 3.16d even a possible ongoing uptake process can be observed.

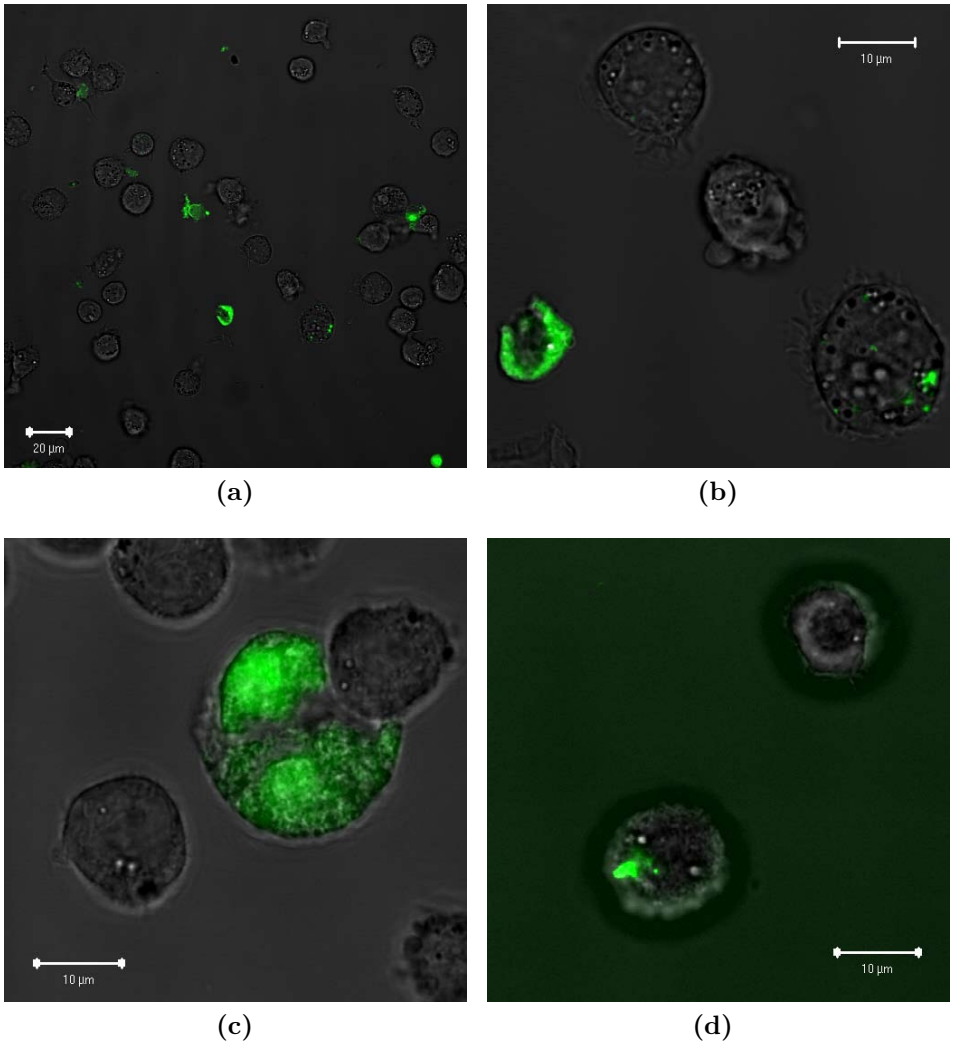

(a) **(b)**

(c) **(d)**

Figure 3.16: THP-1 internalization of alexa488 labeled PB-siDNA self-assemblies, imaged by CLSM.

PB-siDNA was labeled using alexa488 dye. We induced self-assembly in doubly distilled filtered water with alexa488 dye. Using this approach the vesicles incorporate the dye. The remaining alexa488 dye in solution was removed using dialysis cassettes with 3500 MWCO (see section 2.4). After labeling and purification the THP-1 cells (130000 $cells \cdot m\ell^{-1}$) were incubated with the PB-siDNA solution for an hour. The samples were then transferred into a 6-well plate and observed using CLSM (see section 2.12).
The result gained from CLSM, especially image 3.16d, indicates that the self-assembled polymer was not properly separated from the remaining dye in solution, as one can see by looking at the fluorescent medium. This was also confirmed by imaging THP-1 cells with an additive of alexa488 dye in doubly distilled water (data not shown).
In order to purify the labeled polymer solution from the dye, we performed a SEC using Sephadex©G-50 and buffer with 150 mM NaCl and 0.01% Azide. To remove the salt of the buffer another dialysis was carried out. The resuling PB-siDNA solution was then

added to the THP-1 cells and incubated for an hour an observed by CLSM afterwards (see figure 3.17).

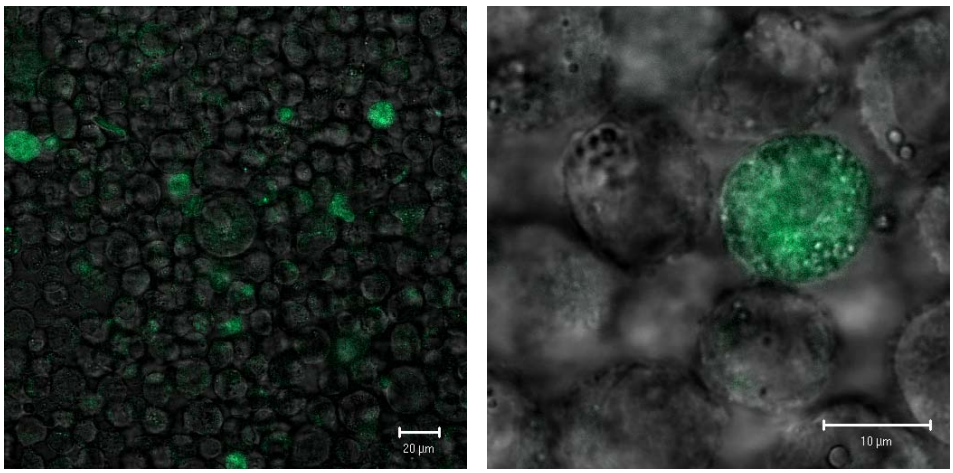

(a) **(b)**

Figure 3.17: THP-1 internalization of alexa488 labeled and SEC purified PB-siDNA self-assemblies, imaged by CLSM.

The data shown in figure 3.17 indicates also an internalization of PB-siDNA into THP-1 cells. Compared to figure 3.16 the dye can be observed as individual dots coming most probably from the labeled PB-siDNA. Unfortunately control experiments of the cells without additive showed that they are fluorescent active at a wavelength of 488 nm. Further studies concluded that the THP-1 medium (see section 2.13) is fluorescent at 488 nm and due to that, the data of the internalization study not very meaningful.
In order to avoid this problem one should wash the cells to remove the fluorescent medium. Due to the lack of time this could not be performed.

CHAPTER 4

Conclusion and Outlook

This master's thesis presents a solid phase synthesis of a biologically active nucleotide-based block copolymer according to Teixeira et al. [13]. As the hydrophilic biologically active segment we used a DNA sequence (*3'*-AACTGAGATGGCGGATGAAGG-*5'*) reported by Luyet et al. [19] which is necessary for infection by the vesicular stomatitis virus. The hydrophobic part consists of *poly*(butadiene), chosen due to its low polydispersity and terminal modification, which is an essential prerequisite to link the hydrophilic and the hydrophobic parts via an amide bond.
The characterization of PB-siDNA by FTIR confirmed the amide linkage with absorbtion bands at 1530 cm^{-1} (δ_{N-H}) and 1634 cm^{-1} ($\nu_{C=O}$). Further, the sugar backbone of the DNA can be seen very clearly. To determine the concentration of PB-siDNA in solution UV/Vis spectroscopy was performed at dilution up to $^1/_{254}$ of stock. An UV absorbtion maximum at 256 nm is a second independent indication for bound nucleotides in the copolymer. Additionally, CD spectroscopy proves the presence of bound DNA with a secondary structure in its A-form with its chiral centers and the right handed helix [16]. Concentration dependant measurements as well as comparisons with the free oligonucleotide would be necessary to make further assumptions on the structure with CD spectroscopy.
The self-assemblies of PB-siDNA were analyzed using DLS, SEM and AFM. SEM images do not really provide significant results due to bad sputtering and aged samples on which the copolymer is mainly forming aggregates. AFM on the other hand could prove the presence of self-assembled vesicles via the phase image, where we could see the cavity inside the vesicles as a change in phase. A radius R_M of 65 nm for an individual structure was calculated via the circumference of the elliptic shape of PB-siDNA gained from the height image. DLS results in a R_h of 88 ± 11 nm for an individual vesicle. Since R_h is expected to be bigger than R_M, because it includes both solvent (*hydro*) and shape (*dynamic*) effects, the radius gained from AFM (R_M) can be compared with the one from DLS (R_h). This should be still applicable if we take the effect of charged systems into account which usually show a smaller hydrodynamic radius (see section 2.8.1). In order to ensure the size and the shape of the self-assembled vesicles one should perform salt-dependant light scattering experiments to neglect charge effects. Further, one could think of performing SLS to make assumptions on the morphology of the self-assemblies.

In order to compare PB-siDNA with a biologically inert system for cell experiments, we used PB-PEG and characterized it with GPC, DLS/SLS and TEM. This copolymer was synthesized in the group of Axel Müller in Bayreuth. GPC was performed with PB standards in chloroform and yielded in a PDI of 1.03 with a M_n of 6500 $g \cdot mol^{-1}$. DLS yields a R_h of 59 ± 4 nm whereas SLS results in a R_g of 80 ± 2 nm. A ρ-factor of 1.35 indicates an elliptic vesicular structure which is also confirmed by TEM experiments. Thus, PB-PEG is a very good biologically inert self-assembled structure for the comparison with PB-siDNA in size as well as in morphology.
Cytotoxicity assays of PB-siDNA and PB-PEG as additives to THP-1 cancer cells indicate a very low toxicity of 5 ± 0.8 % for PB-siDNA and 4 ± 1 % for PB-PEG respectively, compared to the control with 3 ± 0.5 % dead/alive cells. Incubation of THP-1 cancer cells with the biologically active PB-siDNA shows that the growth of THP-1 cells is reduced compared to PB-PEG and to the control. The observation that the PB-siDNA is reducing the cell growth of THP-1 cancer cells without being toxic is very interesting. If the self-assembled PB-siDNA is only targeting cancer cells and has no toxic effect on other (i.e. healthy) cells lines, one could think of using them for cancer therapy. Further experiments (i.e. with other cell lines) are still necessary to clarify if only the growth of cancer cells is affected. Also one could think of using siRNA[1] instead of siDNA to induce RNAi[2] and by that, silencing of particular genes [9, 12].

1 Small Interfering RNA
2 RNA Interference

Acknowledgment

During my master's thesis I had the support of many people. I would like to thank all of them, first of all Dr. Corinne Vebert. She lead me already through a block course and also gave me the opportunity to do a semester work in her group. The introduction and the training I got from her, encouraged me in doing physical chemistry also for my PhD. Thanks are given to Prof. Dr. Wolfgang Meier for the master's examination and the evaluation of the thesis. I thank Nicolas Cottenye, Julia Razumovitch, Kelnner Rodrigues de França and Francisco Teixeira who introduced me to the different techniques as the synthesis of the block copolymer, cell work, FTIR and AFM. Also I am very grateful to Prof. Dr. Axel Müller who provided me with PB-PEG and to Daniel Mathys and Marcel Düggelin from the ZMB who helped me with the SEM and TEM pictures. Further, I'd like to thank Markus Ledergerber, Martin Nussbaumer, Bella Syga, Raphael Urbani, Michael Walther, Johanna Frey and my parents for fruitful discussions. Many thanks are also given to the people I might have forgotten.

Bibliography

1. Baram, M.; Kaplan, W. D.: Quantitative HRTEM Analysis of FIB Prepared Specimens. In: *Journal of Microscopy* 232 (2008), Nr. 3, P. 395–405. (cited on page 10)

2. Barenholz, Y.: Liposome Application: Problems and Prospects. In: *Current Opinion in Colloid & Interface Science* 6 (2001), Nr. 1, P. 66–77. http://dx.doi.org/10.1016/S1359-0294(00)00090-X. (cited on page 1)

3. Binnig, G.; Quate, C. F.; Gerber, C.: Atomic Force Microscope. In: *Physical Review Letters* 56 (1986), Nr. 9, P. 930–933. http://dx.doi.org/10.1103/PhysRevLett.56.930.

4. Byler, D. M.; Susi, H.: Examination of the Secondary Structure of Proteins by Deconvolved FTIR Spectra. In: *Biopolymers* 25 (1986), Nr. 3, P. 469–487. http://dx.doi.org/10.1002/bip.360250307. (cited on page 12)

5. Cantor, C. R.; Warshaw, M. M.; Shapiro, H.: Oligonucleotide Interactions. III. Circular Dichroism Studies of the Conformation of Deoxyoligonucleotides. In: *Biopolymers* 9 (1970), P. 1059–1077. (cited on page 14)

6. Claxton, N. S.; Fellers, T. J.; Davidson, M. W.: *Laser Scanning Confocal Microscopy*, The Florida State University, Technical Report, 2004. (cited on page 16) (cited on page 12)

7. Discher, B. M.; Won, Y.-Y.; Ege, D. S.; Lee, J. C.-M.; Bates, F. S.; Discher, D. E.; Hammer, D. A.: Polymersomes: Tough Vesicles Made from Diblock Copolymers. In: *Science* 284 (1999), Nr. 5417, P. 1143–1145. http://dx.doi.org/10.1126/science.284.5417.1143. (cited on page 1)

8. Discher, D. E.; Eisenberg, A.: Polymer Vesicles. In: *Science* 297 (2002), Nr. 5583, P. 967–973. http://dx.doi.org/10.1126/science.1074972. (cited on page 1)

9. Fire, A.; Xu, S.; Montgomery, M.; Kostas, S.; Driver, S.; Mello, C.: Potent and Specific Genetic Interference by Double-Stranded RNA in Caenorhabditis Elegans. In: *Nature* 391 (1998), Nr. 6669, P. 806–11. http://dx.doi.org/doi:10.1038/35888. (cited on page 34)

10. Förster, S.; Schmidt, M.; Antonietti, M.: Static and Dynamic Light Scattering by Aqueous Polyelectrolyte Solutions: Effect of Molecular Weight, Charge Density

and Added Salt. In: *Polymer* 31 (1990), Nr. 5, P. 781–792. http://dx.doi.org/10.1016/0032-3861(90)90036-X. (cited on page 7)

11. Gong, Y.; Luo, Y.; Bong, D.: Membrane Activation: Selective Vesicle Fusion via Small Molecule Recognition. In: *Journal of the American Chemical Society* 128 (2006), Nr. 45, P. 14430–14431. http://dx.doi.org/10.1021/ja0644576. (cited on page 1)

12. Hammond, S.; Bernstein, E.; Beach, D.; Hannon, G.: An RNA-Directed Nuclease Mediates Post-Transcriptional Gene Silencing in Drosophila Cells. In: *Nature* 404 (2000), Nr. 6775, P. 293–6. http://dx.doi.org/doi:10.1038/35005107. (cited on page 34)

13. Jr., F. T.; Rigler, P.; Vebert, C.: Nucleo-Copolymers: Oligonucleotide-Based Amphiphilic Diblock Copolymers. In: *Chemical Communications Articles* 11 (2007), P. 1130–1132. http://dx.doi.org/10.1039/b617109e. (cited on pages 1, 3, and 33)

14. Kibbe, W. A.: OligoCalc: An Online Oligonucleotide Properties Calculator. In: *Nucleic Acids Research* (Web Server Issue) 35 (2007). http://dx.doi.org/doi:10.1093/nar/gkm234. (cited on pages 15 and 17)

15. Kosloski, M. J.; Rosen, F.; Milholland, R. J.; Papahadjopoulos, D.: Effect of Lipid Vesicle (Liposome) Encapsulation of Methotrexate on Its Chemotherapeutic Efficacy in Solid Rodent Tumors. In: *Cancer Research* 38 (1978), Nr. 9, P. 2848–2853. (cited on page 1)

16. Kypr, J.; Kejnovská, I.; Renčiuk, D.; Vorlíčková, M.: Circular Dichroism and Conformational Polymorphism of DNA. In: *Nucleic Acids Research* 37 (2009), Nr. 6, P. 1713–1725. http://dx.doi.org/doi:10.1093/nar/gkp026. (cited on pages 7, 15, and 33)

17. Ledergerber, M.: *Analysis of Self-Assembled Nucleotide-Based Amphiphilic Block Copolymer Vesicles*, University of Basel, Master's Thesis, 2009. (cited on page 9)

18. Li, S.; Byrne, B.; Welsh, J.; Palmer, A. F.: Self-Assembled *Poly*(Butadiene)-b-*Poly*(Ethylene Oxide) Polymersomes as Paclitaxel Carriers. In: *Biotechnology Progress* 23 (2007), P. 278–285. http://dx.doi.org/10.1021/bp060208. (cited on page 27)

19. Luyet, P.; Falguières, T.; Pons, V.; Pattnaik, A. K.; Gruenberg, J.: The ESCRT-I Subunit Tsg101 Controls Endosometo-Cytosol Release of Viral RNA. In: *Traffic* 9 (2008), P. 2279–2290. http://dx.doi.org/10.1111/j.1600-0854.2008.00820.x. (cited on pages 1, 27, and 33)

20. McPhie, P.: Dialysis. In: *Methods Enzymol* 22 (1971), P. 23–33. (cited on page 5)

21. Mysels, K. J.: Charge Effects in Light Scattering by Colloidal Solutions. In: *The Journal of Physical Chemistry* 58 (1954), Nr. 4, P. 303–207. http://dx.doi.org/10.1021/j150514a004. (cited on page 7)

22. Nardin, C.; Widmer, J.; Winterhalter, M.; Meier, W.: Amphiphilic Block Copolymer Nanocontainers as Bioreactors. In: *The European Physical Journal*

E 4 (2001), Nr. 4, P. 403–410. http://dx.doi.org/10.1007/s101890170095. (cited on page 1)

23. Raman, K.; Schor, R.: Effects of Ionic Charge on Light Scattering by Macromolecules in Solution. In: *The Journal of Chemical Physics* 66 (1977), Nr. 5, P. 1837–1841. http://dx.doi.org/10.1063/1.434181. (cited on page 7)

24. Renggli, K.: *Synthesis and Characterization of Janus Micelles*, University of Basel, Project Thesis, 2008. (cited on page 7)

25. Ruska, E.: The Development of the Electron Microscope and of Electron Microscopy. In: *Nobel lecture* (1986). (cited on page 10)

26. Schmitz, K. S.: *An Introduction to Dynamic Light Scattering by Macromolecules*. Academic Press, Inc., 1990. (cited on page 7)

27. Schurr, J. M.; Schmitz, K. S.: Dynamic Light Scattering Studies of Biopolymers: Effects of Charge, Shape, and Flexibility. In: *Annual Review of Physical Chemistry* 37 (1986), Nr. 1, P. 271–305. http://dx.doi.org/10.1146/annurev.pc.37.100186.001415. (cited on page 7)

28. Sessa, G.; Weissmann, G.: Phospholipid Spherules (Liposomes) as a Model for Biological Membranes. In: *Journal of Lipid Research* 9 (1986), P. 310–318. (cited on page 1)

29. Stengel, G.; Zahn, R.; Höök, F.: DNA-Induced Programmable Fusion of Phospholipid Vesicles. In: *Journal of the American Chemical Society* 129 (2007), Nr. 31, P. 9584–9585. http://dx.doi.org/10.1021/ja073200k. (cited on page 1)

30. Tataurov, A. V.; You, Y.; Owczarzy, R.: Predicting Ultraviolet Spectrum of Single Stranded and Double Stranded Deoxyribonucleic Acids. In: *Biophysical Chemistry* 133 (2008), P. 66–70. (cited on pages 16 and 17)

31. Tsuchiya, S.; Yamabe, M.; Yamaguchi, Y.; Kobayashi, Y.; Konno, T.; Tada, K.: Establishment and Characterization of a Human Acute Monocytic Leukemia Cell Line (THP-1). In: *International Journal of Cancer* 26 (1980), Nr. 2, P. 171–176. (cited on pages 2, 13, 27, and 30)

32. Wilson, T.; Papahadjopoulos, D.; Taber, R.: The Introduction of Poliovirus RNA into Cells via Lipid Vesicles (Liposomes). In: *Cell* 17 (1979), Nr. 1, P. 77–84. http://dx.doi.org/10.1016/0092-8674(79)90296-4. (cited on page 1)

33. Young, R. J.; Lovell, R. A.: *Introduction to Polymers*. 2^{nd} Edition, CRC Press, 1991. (cited on pages 5, 6, and 7)

List of Figures

List of Tables

Glossary

AFM Atomic Force Microscopy

CD Circular Dichroism

CLSM Confocal Laser Scanning Microscopy

DCM Dichloromethane

DIC Diisopropylcarbodiimide

DLS Dynamic Light Scattering

DNA Desoxyribonucleic Acid

FTIR Fourier Transform Infrared Spectroscopy

GPC Gel Permeation Chromatography

HV High Voltage

MWCO Molecular Weight Cut-Off

PB *Poly*(Butadiene)

PDI Polydispersity Index

PEG *Poly*(Ethylene-Glycol)

PEO *Poly*(Ethylene-Oxide)

RNAi RNA Interference

RPM Rounds per Minute

SEC Size Exclusion Chromatography

SEM Scanning Electron Microscopy

siDNA Small Interfering DNA

siRNA Small Interfering RNA

SLS Static Light Scattering

TEM Transmission Electron Microscopy

THF Tetrahydrofuran

UV Ultraviolet

APPENDIX A

GPC Calibration

lg Mp	Mp [$^g/_{mol}$]	Volume [$m\ell$]	Volume^2	Volume^3	Volume^4	Volume^5
4.260071388	18200	6.080	36.966400	224.7557120	1366.514729	8308.40955
4.260071388	18200	6.082	36.990724	224.9775834	1368.313662	8322.08369
4.127104798	13400	6.239	38.925121	242.8538299	1515.165045	9453.11471
4.127104798	13400	6.245	39.000025	243.5551561	1521.001950	9498.65717
3.803457116	6360	6.808	46.348864	315.5430661	2148.217194	14625.06266
3.803457116	6360	6.809	46.362481	315.6821331	2149.479644	14635.80690
3.562292864	3650	7.183	51.595489	370.6103975	2662.094485	19121.82469
3.562292864	3650	7.185	51.624225	370.9200566	2665.060607	19148.46046
3.330413773	2140	7.518	56.520324	424.9197958	3194.547025	24016.60453
3.330413773	2140	7.517	56.505289	424.7502574	3192.847685	24000.63605
3.075546961	1190	8.018	64.288324	515.4637818	4132.988603	33138.30262
3.075546961	1190	8.017	64.272289	515.2709409	4130.927133	33117.64283

Table A.1: GPC calibration data for chloroform

A.1 Calibration Constants

A	B	C	D	E	F
-0.0672688	2.5443690	-38.2002087	284.7298574	-1054.7453830	1559.3695560
0.0141801	0.4950076	6.8955112	47.9140400	166.0778364	229.7290753
0.9999941	0.0014265	#NV	#NV	#NV	#NV

Table A.2: GPC calibration constants for chloroform

APPENDIX B

Raw Data of the Cell Experiments

Raw data of the experiments with THP-1 cells. The concentration $[cells \cdot m\ell^{-1}]$ is calculated using the equation for Neubauer improved, where N_n corresponds to the number of cells in a quadrant of the counting chamber.

$$c = \frac{N_1 + N_2 + N_3 + N_4 + N_5}{5} \cdot 10^4 \tag{B.1}$$

For the cytotoxicity assays the concentration has to be multiplied by two because we count a solution with equal amounts of Trypan blue and cells.

Table B.1: Raw data of cell counting after 120 hours of incubation

Well	N_1	N_2	N_3	N_4	N_5
control $1a$	93	98	100	79	97
control $1b$	79	103	91	89	92
control $2a$	98	73	79	92	84
control $2b$	85	79	87	-	93
2 μM *PB-siDNA* $1a$	63	65	57	104	71
2 μM *PB-siDNA* $1b$	82	71	-	55	93
2 μM *PB-siDNA* $2b$	78	88	93	102	68
2 μM *PB-PEG* $1a$	76	95	83	78	95
2 μM *PB-PEG* $1b$	106	86	98	78	75
2 μM *PB-PEG* $2a$	83	109	78	61	92
2 μM *PB-PEG* $2b$	92	103	93	85	75
1 μM *PB-siDNA* $1a$	-	109	75	98	-
1 μM *PB-siDNA* $1b$	73	45	56	-	65
1 μM *PB-siDNA* $2a$	73	58	75	81	71
1 μM *PB-siDNA* $2b$	62	71	73	85	78
1 μM *PB-PEG* $1a$	112	-	106	109	85
1 μM *PB-PEG* $1b$	93	78	112	78	79

continued on next page

1 μM PB-PEG $2a$	46	63	52	78	58
1 μM PB-PEG $2b$	93	95	123	120	79
500 nM PB-siDNA $1a$			Error		
500 nM PB-siDNA $1b$	63	59	83	72	78
500 nM PB-siDNA $2a$	67	78	75	64	68
500 nM PB-siDNA $2b$	78	65	78	85	71
500 nM PB-PEG $1a$	68	53	68	57	72
500 nM PB-PEG $1b$	87	104	97	87	76
500 nM PB-PEG $2a$	102	95	90	-	98
500 nM PB-PEG $2b$	101	81	93	100	78
100 nM PB-siDNA $1a$	65	-	72	56	68
100 nM PB-siDNA $1b$	78	56	55	75	48
100 nM PB-siDNA $2a$	51	57	70	78	71
100 nM PB-siDNA $2b$	75	78	55	54	71
100 nM PB-PEG $1a$	98	68	92	92	48
100 nM PB-PEG $1b$	81	71	93	78	93
100 nM PB-PEG $2a$	78	95	109	98	102
100 nM PB-PEG $2b$	78	98	104	78	109